PHYSICAL REVIEW A VOLUME 24, NUMBER 2 AUGUST 1981

K-shell ionization by low-velocity ions

R. K. Rice,* F. D. McDaniel, G. Basbas,† and J. L. Duggan
Department of Physics, North Texas State University, Denton, Texas 76203
(Received 17 February 1981)

K-shell x-ray–production measurements are reported for protons, deuterons, and alpha particles incident on thin foils of copper, niobium, silver, and antimony. In the velocity range of the experiments, which correspond to 100–600 keV/u, the energy of ionization was as large as 10% of the bombarding energy. The inferred dependence of the excitation process on the projectile mass, atomic number, and energy is compared with theoretical estimates of a low-velocity ionization threshold, the binding effect, and the Coulomb-deflection effect. Precision of measurement is not great enough to discern unambiguously the threshold effect but the binding and Coulomb-deflection effects are clearly distinguished.

I. INTRODUCTION

In recent years low-velocity ion beams have come into increasing use in a variety of new areas of research; examples include surface physics, ion implantation, and plasma heating. The ion velocities, typically on the order of an atomic unit ($v_0 = e^2/\hbar = 2.2\times10^8$ cm/sec), are much lower than the average velocity of inner-shell electrons in many of the target materials. They approach the conservation-of-energy threshold in the inelastic collisions which are responsible for K-shell ionization and other inner-shell excitations. In the case of electron bombardment, the ionization threshold has been studied and can manifest itself in other phenomena, for example, ion desorption via the Auger decay of an inner-shell vacancy.[1]

In contrast, it is not known how or if the excitation threshold under ion bombardment will affect other phenomena. It is only recently that inner-shell ionization at low energies has begun to be examined for a threshold effect.[2-4] One of the purposes of this work is to examine this phenomenon.

The usual methods of detecting inelastic collisions via x-ray or Auger-electron production give very small signals at low bombarding velocities. As a result the cross sections inferred typically have an uncertainty which makes difficult the delineation of the various physical mechanisms which influence the excitation or ionization process. Influences upon ionization at low velocities have previously been attributed to a binding effect and a Coulomb-deflection effect.[5,6] To our knowledge, no one has exploited secondary phenomena, such as ion desorption, to obtain low-velocity measurements with improved precision.

In the work reported here, we examine, as carefully as our instruments will allow, the behavior of the K-shell ionization process under ion bombardment at low velocities. We report measurements of K-shell x-ray production and study the dependence of this process on projectile mass, atomic number, and energy. The experiments were conducted for protons ($^1_1$H), deuterons ($^2_1$D), and alpha particles ($^4_2$He) incident on thin solid foils of $_{29}$Cu, $_{41}$Nb, $_{47}$Ag, and $_{51}$Sb of various thicknesses. Cross sections were inferred at projectile energies corresponding to a variation from 100 to 600 keV/u.

The reasons for using these three projectiles are as follows:

(1) Protons and deuterons have the same nuclear charge Z_1e and different masses. At the same velocity, therefore, they have the same increased binding effect and different Coulomb-deflection effects. By forming ratios of measured cross sections the Coulomb-deflection effect can be isolated.

(2) Deuterons and alpha particles have the same charge to mass ratio and, therefore, at the same velocity they have the same Coulomb-deflection effect. Their different charges produce different binding effects. By forming ratios of measured cross sections, the increased binding effect can be isolated.

Forming these ratios of cross sections allows the cancellation of some calibration quantities. The ratio values thereby become more accurate quantities than absolute cross section measurements. Typical uncertainties of cross-section measurements are 10–15%. Published values from different experimenters, however, can differ by much more than this.[7] Ratios have uncertainties of about 7%.

The threshold aspect of this work focuses on the assumption $\hbar\omega_{2K}/E_{\text{c.m.}} \ll 1$ commonly employed in calculating K-shell ionization cross sections in the plane-wave Born approximation (PWBA).[8-10]

Here $\hbar\omega_{2K}$ is the observed binding energy of the K shell[11] and $E_{\text{c.m.}}$ is the total energy in the center-of-mass system ($E_{\text{c.m.}} = \frac{1}{2}Mv_1^2$), where M is the reduced mass of the incident particle-target nucleus system. The assumption manifests itself in the use of approximate limits of integration.[9] A consequence of this assumption, made for convenience, is the unphysical prediction of a nonvanishing cross section for any projectile energy, however small. Avoiding this assumption produces a threshold for ionization at $E_{\text{c.m.}} = \hbar\omega_{2K}$.

This threshold effect is examined theoretically in the present paper by calculating cross sections in the PWBA and perturbed stationary state (PSS)[5] theories with both the exact and approximate limits of integration in the projectile energy region corresponding to $\hbar\omega_{2K}/E_{\text{c.m.}} \leq 0.1$. Two Coulomb-deflection factors (C_K and C_B)[5,6] and two relativistic corrections (R_A and R_B)[12,13] were also included in the calculations.

II. THEORY

A. Background

The PWBA is a quantum mechanical description of inner-shell ionization by fast ions formulated in 1930 by Bethe.[8] In the transition matrix elements the exact eigenfunction is replaced by the product of a plane wave and an unperturbed atomic state. The PWBA is considered to be valid for the ionization process if the incident ion is in the high velocity range, where $(Z_1e^2/\hbar v_1) \ll 1$, so that the initial and final particle states can be treated as plane waves, and if the atomic number of the incident ion Z_1 is much less than the atomic number of the target Z_2, so that the ionizing interaction is weak.

The doubly differential cross section in the center-of-mass system for a transition from the initially filled K shell to the continuum with energy transfer $WZ_{2K}^2\mathcal{R}$ and momentum transfer $\hbar Q^{1/2}/a_{2K}$ is given by[9]

$$d^2\sigma_{WK} = 8\pi Z_1^2\left(\frac{e^2}{\hbar v_1}\right)\frac{dQ}{Q^2}|F_{WK}(Q)|^2\,dW\,a_{2K}^2. \tag{1}$$

We describe the electron states by hydrogenic wave functions. The square of the form factor summed over angles of electron ejection, $|F_{WK}(Q)|^2$, is obtained in closed form.[9] Here, v_1 is the relative velocity between the projectile and target $[v_1 = (2E_1/M_1)^{1/2}]$, E_1 is the incident energy in the laboratory, M_1 is the projectile mass, Z_1e is the charge of the incident projectile, a_0 is the Bohr radius of hydrogen, $a_{2K} = a_0/Z_{2K}$, $\mathcal{R}$ denotes the Rydberg constant, and $Z_{2K}e = (Z_2 - 0.3)e$ is a screened charge[14] for the target nucleus.

The differential cross section per interval of energy transfer can now be obtained by integrating Eq. (1) over the momentum transfer variable Q. The limits of the integration are established from conservation of energy. The assumption $\hbar\omega_{2K}/E_{\text{c.m.}} \ll 1$ is usually introduced in evaluating these limits. The limits are denoted by $Q_{\min}$ and $Q_{\max}$.

The integration over Q yields the excitation function[9] $I_K(W)$, given by

$$I_K(W) = \int_{Q_{\min}}^{Q_{\max}} |F_{WK}(Q)|^2\,\frac{dQ}{Q^2}. \tag{2}$$

The K-shell differential energy transfer cross section is now given by

$$d\sigma_K = 8\pi Z_1^2 a_0^2 Z_{2K}^{-4}\eta_K^{-1} I(W)dW, \tag{3}$$

$$\eta_K = \left(\frac{v_1}{Z_{2K}v_0}\right)^2 = \frac{m}{M_1}\,\frac{E_1}{Z_{2K}^2\mathcal{R}} = \frac{m}{M}\,\frac{E_{\text{c.m.}}}{Z_{2K}^2\mathcal{R}}. \tag{4}$$

Here, $v_0 = e^2/\hbar$, m is the electron mass, M is the reduced mass of the incident ion-target nucleus system, and $E_1/M_1 = E_{\text{c.m.}}/M$ as in Ref. 9. Equation (3) is integrated to give the total direct Coulomb ionization cross section for the K shell, σ_K,

$$\sigma_K = 8\pi Z_1^2 a_0^2 Z_{2K}^{-4}\eta_K^{-1}\int_{\theta_K}^{W_{\max}} I_K(W)dW, \tag{5}$$

where θ_K corresponds to the minimum energy transferred, and is defined as

$$\theta_K = \hbar\omega_{2K}/(Z_{2K}^2\mathcal{R}). \tag{6}$$

θ_K may also be viewed as a screening number since it is the ratio of the observed ionization potential of the K-shell ($\hbar\omega_{2K}$) to the ideal ionization potential without outer screening, $Z_{2K}^2\mathcal{R}$. θ_K has values between 0.5 and 1.0. The maximum energy transferred is denoted by $W_{\max}$.

It is customary[10] to define

$$f_K(\eta_K, \theta_K) = \int_{\theta_K}^{W_{\max}} I_K(W)\,dW \tag{7}$$

and

$$\sigma_{0K} = 8\pi Z_1^2 a_0^2 Z_{2K}^{-4}, \tag{8}$$

and to express the total cross section as

$$\sigma_K = \sigma_{0K}\eta_K^{-1} f_K(\eta_K, \theta_K). \tag{9}$$

It has been shown[5] that the cross sections exhibit an almost universal behavior when $\theta_K f_K/\eta_K$ is plotted as a function of the single variable η_K/θ_K^2 in the low-velocity region. By defining

$$F_K(\eta_K/\theta_K^2, \theta_K) = (\theta_K/\eta_K) f_K(\eta_K, \theta_K), \tag{10}$$

the total cross section can now be written as

$$\sigma_K = \sigma_{0K}\theta_K^{-1} F_K(\eta_K/\theta_K^2, \theta_K). \tag{11}$$

The universal function $F_K(\eta_K/\theta_K^2, \theta_K)$ also has a parametric dependence on θ_K.

B. Evaluation of the limits of integration

The energy conservation condition limits the momentum transfer variable q as follows[9]:

$$(\hbar q_{\min})^2 = 2M[(E_{\text{c.m.}})^{1/2} - (E_{\text{c.m.}} - \epsilon)^{1/2}]^2 = \hbar^2 Q_{\min}/a_{2K}^2 \quad (12)$$

and

$$(\hbar q_{\max})^2 = 2M[(E_{\text{c.m.}})^{1/2} + (E_{\text{c.m.}} - \epsilon)^{1/2}]^2 = \hbar^2 Q_{\max}/a_{2K}^2 , \quad (13)$$

where $\hbar q$ is the magnitude of the momentum transferred, ϵ is the energy transferred, and M is the reduced mass of the projectile-target system. Converting these expressions to the variables η_K, $W = \epsilon/Z_{2K}^2 \mathcal{R}$, and Q defined earlier, the following is obtained:

$$Q_{\min} = \rho^2 \eta_K \{1 - [1 - (W/\rho\eta_K)]^{1/2}\}^2 \quad (14)$$

and

$$Q_{\max} = \rho^2 \eta_K \{1 + [1 - (W/\rho\eta_K)]^{1/2}\}^2 , \quad (15)$$

where $\rho = M/m$, and we have made use of the fact that $E_1/M_1 = E_{\text{c.m.}}/M$ as pointed out in Ref. 9.

If $\epsilon \ll E_{\text{c.m.}}$, or $W/\rho\eta_K \ll 1$, which requires $\hbar\omega_{2K} \ll E_{\text{c.m.}}$, then $Q_{\min}$ can be written for all practical purposes[9] as

$$Q_{\min} = W^2/4\eta_K . \quad (16)$$

Similarly $Q_{\max}$ can be set equal to infinity.

For the W integration, $W_{\max}$ was set equal to $\rho\eta_K$ since the energy transferred cannot exceed the energy of the incident particle in the center-of-mass system. However, for most purposes $W_{\max}$ can be taken as infinite.[9]

Values of $f_K(\eta_K, \theta_K)$ calculated using the approximate limits of integration have been tabulated by Khandelwal, Choi, and Merzbacher.[10] Values of $F_K(\eta_K/\theta_K^2, \theta_K)$ have been published[15] for an extended range of η_K/θ_K^2 and θ_K values, also using the approximate limits of integration. In the present paper we calculate $F_K(\eta_K/\theta_K^2, \theta_K)$ with exact limits.

In the remainder of this work the notation PWBA (exact) and PWBA will be used to distinguish between calculations with exact and approximate limits, respectively. The use of the exact limits introduces a dependence on the mass through the variable ρ and therefore cross sections cannot be tabulated easily. The cross-section ratio PWBA (exact)/PWBA is plotted in Fig. 1 for protons incident on $_{29}$Cu versus $\mu = \hbar\omega_{2K}/E_{\text{c.m.}}$. The upper scale gives the incident energy in keV. It should be noted that for small μ the cross-section ratio approaches unity. This is where the

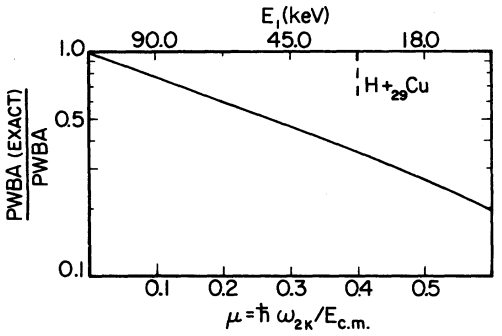

FIG. 1. Ratio of PWBA(exact) to PWBA for protons on $_{29}$Cu versus $\mu = \hbar\omega_{2K}/E_{\text{c.m.}}$. The upper scale gives the energy in keV for protons incident on $_{29}$Cu.

K-shell binding energy is much less than $E_{\text{c.m.}}$ as required for the validity of the approximate limits. The ratio reaches approximately 0.75 for $\mu = 0.1$. Details of the actual numerical integration and tabulated values of the cross-section ratios can be found elsewhere.[16]

The inclusion of the effects of increased binding of the K-shell electron and the polarization of the electron orbit by the projectile outlined elsewhere[5,17] have been shown to help explain the results of experiments.[18-25] The cross section which includes these effects has its origin in the PSS theory but for convenience is cast in terms of the PWBA with reduced variables giving

$$\sigma_K(\text{PSS}) = (\sigma_{0K}/\zeta_K\theta_K) F(\eta_K/(\zeta_K\theta_K)^2, \zeta_K\theta_K), \quad (17)$$

where ζ_K, discussed in the last citations of Ref. 5, represents the inclusion of increased binding and polarization effects. In calculations used in this work the polarization effects are negligible but the PSS calculation was used for the sake of completeness in obtaining the "best" theoretical description available.

An approximate correction for the Coulomb deflection of the incident projectile by the target nucleus given by Brandt *et al.*[5] (C_B) is applied as a multiplicative factor to the PWBA and PSS theories. Another Coulomb-deflection calculation by Kocbach[6] (C_K) can also be incorporated accurately as a multiplicative factor given by Anholt.[26] Both of these Coulomb-deflection factors are given as functions of the variable $\pi d q_0 = \frac{1}{2}\pi Z_1 (m/M)\theta_K^{-2} \times (\eta_K/\theta_K^2)^{-3/2}$, where $d = \frac{1}{2}(Z_1 Z_2 e^2/\frac{1}{2}Mv_1^2)$ is the half distance of closest approach in a head-on collision and is the optimum penetration distance for K-shell ionization. $q_0 = q_{\min}$ as defined in Eq. (12) with $\epsilon = \hbar\omega_{2K}$. Here, unlike the usual treatment, we use exact limits in calculating the Coulomb-deflection effect.

Finally, relativistic effects become important for high-Z_2 targets, where the K-shell electron

velocities approach the speed of light. Both Anholt[12] and Brandt and Lapicki[13] give methods for incorporating relativistic effects into the predictions of the PWBA and PSS theories. These two calculations, R_A (Anholt) and R_B (Brandt) have been incorporated into the theoretical calculations presented in this work.

III. EXPERIMENTAL PROCEDURE

The incident beams of $^1_1$H, $^2_1$D, and $^4_2$He ions were produced by the High Voltage Engineering Corporation 2.5-MV Van de Graaff Accelerator at the Regional Atomic and Nuclear Physics Laboratory at North Texas State University. The ion beams were energy and mass analyzed to an accuracy of 1% by a calibrated bending magnet. The analyzed beam was collimated by two 2-mm-diameter tantalum apertures located approximately 75 cm before the target chamber and by a 3-mm-diameter carbon aperture at the entrance of the target chamber. The targets were mounted on a ladder which was rotated to position the targets at 45° to the incident beam. The targets ranged in thickness from 16 to 200 μg/cm^2. Some were self-supporting and others were mounted on 10–50-μg/cm^2 carbon backings. Thicknesses, listed in Table I, were measured using Rutherford scattering with 1–2-MeV protons at an angle of 150°. Calculated target thickness uncertainties are ± 7% due to counting statistics, source calibration, solid angle measurement, and beam-energy uncertainties. An ORTEC intrinsic Ge detector with a resolution of 225 eV full width at half maximum (FWHM) at 5.9 keV was positioned inside the target chamber approximately 2 cm from the target and at 90° to the incident-beam direction. A Si surface-barrier detector was mounted at 150° to the incident beam direction to detect the Rutherford elastically scattered particles from the target. After passing through the target, the incident particles were collected in a Faraday cup behind the chamber which was equipped with a − 300 V electron suppressor to allow accurate current integration.

TABLE I. Target thicknesses.

Element	Z_2	Thickness[a] (μg/cm^2)
Cu	29	47.1
		68.3
		155.0 (SS)[b]
Nb	41	16.5
		25.3
		58.7
Ag	47	82.0 (SS)
		131.0 (SS)
		152.0 (SS)
Sb	51	61.2
		207.0

[a] The target thicknesses given were measured with the target positioned in the beam at an angle of 45° with respect to the incident beam direction.

[b] (SS) indicates self-supporting targets, all others were mounted on 10–50-μg/cm^2 carbon foils.

The Ge detector was calibrated for efficiency and solid angle using calibrated sources of ^{65}Zn, ^{155}Eu, and ^{241}Am by procedures described in the literature.[27] A 0.66-mm Mylar foil was placed between the target and the beryllium window of the detector to suppress low-energy L-shell x rays and to keep scattered particles from entering the x-ray detector.

The Si surface-barrier detector was equipped with a 1-mm collimator to prevent high count rates from the large Rutherford scattering cross sections at low incident energies. The surface-barrier detector had a FWHM energy resolution of 18 keV and was calibrated for energy as well as for efficiency and solid angle using a calibrated ^{244}Cm source. Since the efficiency of the Si surface-barrier detector is 100% for ions at these energies, the calibrated ^{244}Cm allowed the solid angle of the detector to be measured and an absolute x-ray cross section to be determined by normalizing the x-ray yield to the Rutherford scattered ion yield. This normalization procedure assumes that the ion scattering is entirely Rutherford in nature and that the mass dependence in the Rutherford differential cross sections is small. For the ions, targets, and scattering angle of the present experiment, the mass dependence reduces the Rutherford cross section by less than 0.7%. This normalization technique has been discussed in detail previously.[19,21,25]

The x-ray and elastically scattered particle spectra were stored in 1024 channels of a multichannel analyzer. Beam currents of $\leq$ 150 nA were used to keep dead time corrections to 2% or less. After background subtraction was performed, x-ray and scattered particle yields were extracted from the respective spectra.

To ensure that detector geometries and target thicknesses did not change from one projectile to the next, each target was bombarded by all three projectiles before being moved. For each element data was taken for several different target thicknesses so that any dependence on thickness could be determined. It was found that a relatively simple energy-loss correction[28] was adequate to correct both x-ray and scattered particle yields for target thickness effects.

IV. DATA ANALYSIS

K-shell x-ray production cross sections were deduced from measured quantities as discussed in previous works[19,21,25] and will not be discussed in detail here. It should be noted, however, that a correction to the x-ray and Rutherford yields to compensate for energy loss in the target foil was applied.[28] This correction has the form $(1-\langle\Delta E_1\rangle/E_1)^{-(s+2)}$, where $\langle\Delta E_1\rangle$ is the average energy loss in passing through the target foil calculated from stopping powers[29] and target thicknesses and s is the slope of the natural log (ln) of the cross-section curve as a function of E_1.

Because of the large values of s encountered in the energy region studied ($3<s<7$) and the large energy losses encountered for low-energy ions passing through the thickest foils ($\langle\Delta E\rangle/E \leq 0.075$), values of this correction factor were as large as a factor of 2. The cross sections exhibited no thickness dependence except for this energy-loss correction. The contribution of electron capture was negligibly small compared to direct ionization.

Sources of experimental uncertainty are tabulated in Table II. The largest uncertainty in the x-ray cross section derives from the strong energy dependence of the cross section

$$Y \propto \sigma_x \propto E_1^s ,$$

so

$$\frac{dY}{Y} = s\,\frac{dE_1}{E_1} , \tag{18}$$

where dE_1/E_1 is the uncertainty in the incident projectile energy. Thus, with s as large as 7 and $dE_1/E_1 = 0.01$, uncertainties of 7% in the measured x-ray yield for incident energy E_1 could be introduced. Owing to lack of calibration points for the magnet system in the low-energy region (< 0.16 MeV) this uncertainty may be even larger for the lowest values of E_1 due to the extrapolation of the energy calibration into this region (expect $dE_1/E_1 < 0.02$ at 0.1 MeV). This only affects the data for protons on $_{29}$Cu below 160 keV and introduces the possibility for relative errors of 15% and absolute errors of 17%.

V. DISCUSSION

The K-shell x-ray production cross sections inferred from measured yields for incident protons, deuterons, and alpha particles are presented in Tables III to V, respectively. Also tabulated are values of the PSS theory calculated with exact limits of integration, Coulomb-deflection effects (C_K and C_B), and relativistic effects (R_A and R_B). These theoretical values have been converted from ionization to x-ray production cross sections using the fluorescence yield values (ω_K) of Bambynek *et al.*[30] The fluorescence yields used are for single-hole vacancies and should be valid under the conditions of all our experiments. Figures 2 and 3 show comparisons of theoretical and measured values of absolute x-ray production cross sections for all three projectiles incident on $_{29}$Cu and $_{47}$Ag, respectively. Measured values from other works[2,18,31-37] are also shown. For $_{29}$Cu the agreement with previously published results is usually within experimental uncertainties. For $_{47}$Ag, however, there are large differences between the present data and some of the previously published results.[2,34,37]

Theoretical calculations employed the exact limits of integration. The four different theoretical curves represent the PSS including combinations of the two Coulomb-deflection calculations (C_K and C_B) and the two relativistic corrections (R_A and R_B) discussed earlier. The effect of the two relativistic calculations is almost identical; Anholt's calculation gives slightly lower values at the lowest energies, with the difference being larger for larger Z_2 and Z_1. The largest difference between the relativistic treatments is ~ 30% for the $^4_2$He on $_{51}$Sb at 0.2 MeV/u.

The results of the two calculations for the Coulomb-deflection effects are quite different. Although they converge at the highest energies for

TABLE II. Experimental uncertainties.

Source	Range
Relative uncertainty	
Counting statistics and background subtraction	
$K\alpha$ and $K\beta$ x-ray yields	1–4%
Back-scattered particle yields	1–4%
Uncertainty in x-ray yield due to uncertainty in incident energy[a]	3–7%
Total relative uncertainty	<9%
Normalization uncertainty	
Absolute efficiency calibration	
Source strength	3%
Source x-ray yields	1–2%
Source relative photon intensities	3%
Particle detector solid angle	5%
Rutherford differential cross section due to uncertainty in angle θ	5%
Total normalization uncertainty	<8.5%
Total absolute uncertainty	<12.4%

[a] This assumes a 1% uncertainty in the incident energy.

TABLE III. Cross sections for K-shell x-ray production by protons (all cross sections are in barns).[a]

E_1/M_1 (MeV/u)	σ_x (measured)	σ_x (C_BPSSR_A)	σ_x (C_KPSSR_A)	σ_x (C_BPSSR_B)	σ_x (C_KPSSR_B)
		Copper ($Z_2=29$, $\omega_K=0.445$)			
0.1	1.37(−4)	2.04(−4)	4.23(−5)	2.20(−4)	4.56(−5)
0.12	5.92(−4)	7.66(−4)	2.47(−4)	8.10(−4)	2.61(−4)
0.14	1.69(−3)	2.08(−3)	8.86(−4)	2.16(−3)	9.19(−4)
0.16	3.82(−3)	4.58(−3)	2.35(−3)	4.70(−3)	2.41(−3)
0.18	7.60(−3)	8.76(−3)	5.13(−3)	8.91(−3)	5.22(−3)
0.20	1.33(−2)	1.52(−2)	9.80(−3)	1.53(−2)	9.86(−3)
0.25	3.91(−2)	4.43(−2)	3.32(−2)	4.43(−2)	3.32(−2)
0.30	8.48(−2)	9.93(−2)	8.07(−2)	9.87(−2)	8.02(−2)
		Niobium ($Z_2=41$, $\omega_K=0.748$)			
0.2	7.07(−5)	9.16(−5)	1.80(−5)	1.07(−4)	2.10(−5)
0.24	3.15(−4)	3.43(−4)	1.06(−4)	3.83(−4)	1.18(−4)
0.28	9.61(−4)	9.24(−4)	3.81(−4)	9.97(−4)	4.11(−4)
0.32	2.14(−3)	2.02(−3)	1.01(−3)	2.13(−3)	1.06(−3)
0.36	4.28(−3)	3.97(−3)	2.28(−3)	3.96(−3)	2.27(−3)
0.40	7.65(−3)	6.63(−3)	4.20(−3)	6.69(−3)	4.24(−3)
0.45	1.39(−2)	1.17(−2)	8.10(−3)	1.17(−2)	8.10(−3)
0.50	2.32(−2)	1.92(−2)	1.42(−2)	1.88(−2)	1.39(−2)
		Silver ($Z_2=47$, $\omega_K=0.83$)			
0.25	1.96(−5)	4.29(−5)	7.03(−6)	5.42(−5)	8.89(−6)
0.30	1.16(−4)	1.68(−4)	4.55(−5)	2.00(−4)	5.41(−5)
0.35	3.75(−4)	4.67(−4)	1.74(−4)	5.29(−4)	1.97(−4)
0.40	1.00(−3)	1.04(−3)	4.79(−4)	1.14(−3)	5.26(−4)
0.45	2.01(−3)	2.00(−3)	1.08(−3)	2.13(−3)	1.15(−3)
0.50	3.64(−3)	3.46(−3)	2.08(−3)	3.62(−3)	2.17(−3)
0.55	6.08(−3)	5.55(−3)	3.62(−3)	5.70(−3)	3.72(−3)
0.60	9.57(−3)	8.40(−3)	5.84(−3)	8.49(−3)	5.91(−3)
		Antimony ($Z_2=51$, $\omega_K=0.867$)			
0.30	1.86(−5)	4.02(−5)	6.84(−6)	5.27(−5)	8.98(−6)
0.35	7.25(−5)	1.26(−4)	3.29(−5)	1.56(−4)	4.07(−5)
0.40	2.03(−4)	3.10(−4)	1.08(−4)	3.64(−4)	1.26(−4)
0.45	5.49(−4)	6.38(−4)	2.72(−4)	7.21(−4)	3.07(−4)
0.50	1.12(−3)	1.16(−3)	5.74(−4)	1.27(−3)	6.33(−4)
0.55	1.82(−3)	1.94(−3)	1.08(−3)	2.08(−3)	1.15(−3)
0.60	3.00(−3)	3.02(−3)	1.82(−3)	3.17(−3)	1.93(−3)
0.65	4.77(−3)	4.47(−3)	2.91(−3)	4.61(−3)	3.00(−3)

[a] The notation 1.37(−4) denotes 1.37×10^{-4}; all theoretical cross sections are the result of integrations with exact limits.

$^4_2$He + $_{29}$Cu, the difference becomes larger for the lighter projectiles and heavier targets at lower energies. Kocbach's calculation is always lower and decreases much more rapidly at lower energies than the calculation of Brandt *et al.*[5] The two calculations differ by a factor of ~ 6 for $^1_1$H on $_{29}$Cu at 0.1 MeV/u. Kocbach's Coulomb-deflection factor is the result of an exact calculation using Rutherford trajectories for protons on Au, whereas Brandt's approximation is the first term in an infinite series of alternating sign.[6,26] Kocbach's calculation gives better results for the high-Z_2 targets but underestimates the measured values for the low-Z_2 targets. This effect has been studied recently by Paul[38] with similar results. Other Coulomb-deflection studies have also been done recently in extended ranges of the variable πdq.[39,40]

In general, the experimental data do not agree with the energy dependence of any of the four theoretical predictions. The majority of the absolute data agree with the C_BPSSR (here $R=R_A$ or R_B since they are practically identical) from the highest energies down to the middle of the energy

TABLE IV. Cross sections for K-shell x-ray production by deuterons (all cross sections are in barns).[a]

E_1/M_1 (MeV/u)	σ_x (measured)	σ_x (C_BPSSR_A)	σ_x (C_KPSSR_A)	σ_x (C_BPSSR_B)	σ_x (C_KPSSR_B)
		Copper ($Z_2=29$, $\omega_k=0.445$)			
0.08	6.90(−5)	2.07(−4)	7.31(−5)	2.24(−4)	7.95(−5)
0.09	2.25(−4)	4.36(−4)	1.89(−4)	4.66(−4)	2.02(−4)
0.10	6.09(−4)	8.12(−4)	4.08(−4)	8.61(−4)	4.32(−4)
0.12	2.03(−3)	2.21(−3)	1.35(−3)	2.30(−3)	1.41(−3)
0.14	4.59(−3)	4.84(−3)	3.35(−3)	4.98(−3)	3.45(−3)
0.16	9.18(−3)	9.14(−3)	6.86(−3)	9.34(−3)	7.01(−3)
0.18	1.63(−2)	1.57(−2)	1.24(−2)	1.59(−2)	1.26(−2)
0.20	2.58(−2)	2.50(−2)	2.07(−2)	2.52(−2)	2.08(−2)
0.25	6.59(−2)	6.39(−2)	5.62(−2)	6.35(−2)	5.59(−2)
0.30	1.45(−1)	1.32(−1)	1.20(−1)	1.30(−1)	1.19(−1)
		Niobium ($Z_2=41$, $\omega_K=0.748$)			
0.16	5.09(−5)	9.91(−4)	3.41(−5)	1.19(−4)	4.07(−5)
0.20	4.63(−4)	3.82(−4)	1.88(−4)	4.33(−4)	2.13(−4)
0.24	1.35(−3)	1.02(−3)	6.17(−4)	1.12(−3)	6.74(−4)
0.28	3.02(−3)	2.15(−3)	1.47(−3)	2.34(−3)	1.60(−3)
0.32	5.60(−3)	4.14(−3)	3.08(−3)	4.30(−3)	3.19(−3)
0.36	1.03(−2)	7.27(−3)	5.73(−3)	7.16(−3)	5.64(−3)
0.40	1.52(−2)	1.12(−2)	9.17(−3)	1.11(−2)	9.14(−3)
0.45	2.35(−2)	1.79(−2)	1.53(−2)	1.80(−2)	1.53(−2)
		Silver ($Z_2=47$, $\omega_K=0.830$)			
0.20	3.06(−5)	5.22(−5)	1.59(−5)	6.71(−5)	2.04(−5)
0.25	1.82(−4)	2.05(−4)	9.30(−5)	2.48(−4)	1.12(−4)
0.30	5.26(−4)	5.58(−4)	3.18(−4)	6.40(−4)	3.64(−4)
0.35	1.33(−3)	1.21(−3)	7.95(−4)	1.34(−3)	8.77(−4)
0.40	2.59(−3)	2.29(−3)	1.64(−3)	2.44(−3)	1.76(−3)
0.45	4.66(−3)	3.87(−3)	2.97(−3)	4.06(−3)	3.11(−3)
0.50	6.64(−3)	6.33(−3)	5.08(−3)	6.29(−3)	5.05(−3)
0.55	1.09(−2)	9.11(−3)	7.58(−3)	9.23(−3)	7.67(−3)
0.60	1.64(−2)	1.30(−2)	1.11(−2)	1.30(−2)	1.11(−2)
		Antimony ($Z_2=51$, $\omega_K=0.867$)			
0.25	4.54(−5)	6.31(−5)	2.15(−5)	8.39(−5)	2.85(−5)
0.30	1.71(−4)	1.88(−4)	8.67(−5)	2.34(−4)	1.08(−4)
0.35	4.27(−4)	4.33(−4)	2.42(−4)	5.12(−4)	2.87(−4)
0.40	8.40(−4)	8.49(−4)	5.40(−4)	9.65(−4)	6.14(−4)
0.45	1.63(−3)	1.49(−3)	1.04(−3)	1.64(−3)	1.14(−3)
0.50	2.82(−3)	2.41(−3)	1.78(−3)	2.58(−3)	1.91(−3)
0.55	4.49(−3)	3.66(−3)	2.85(−3)	3.83(−3)	2.98(−3)
0.60	6.73(−3)	5.28(−3)	4.26(−3)	5.45(−3)	4.40(−3)
0.65	8.50(−3)	7.36(−3)	6.11(−3)	7.47(−3)	6.21(−3)

[a] The notation 6.90(−5) denotes 6.90×10^{-5}; all theoretical cross sections are the results of integrations with exact limits.

range within experimental uncertainties. At this point the data decrease more rapidly than the C_BPSSR and reach the predictions of the C_KPSSR_B at the lowest incident energies. With the exception of the $_{41}$Nb data, this tendency is present for all three projectiles and all four targets. For $_{41}$Nb the experimental data seem high relative to the theoretical predictions but exhibit the same relative energy dependence.

Since the effect of the exact versus approximate limits is small compared to discrepancies between theory and experiment, and since the numerical difference between the two relativistic treatments is also relatively small, it is reasonable

TABLE V. Cross sections for K-shell x-ray production by alpha particles (all cross sections are in barns).[a]

E_1/M_1 (MeV/u)	σ_x (measured)	σ_x (C_BPSSR_A)	σ_x (C_KPSSR_B)	σ_x (C_BPSSR_B)	σ_x (C_KPSSR_B)
		Copper ($Z_2=29$, $\omega_K=0.445$)			
0.08	1.58(−4)	3.93(−4)	1.22(−4)	4.41(−4)	1.37(−4)
0.09	5.83(−4)	8.49(−4)	3.31(−4)	9.38(−4)	3.65(−4)
0.10	1.12(−3)	1.62(−3)	7.43(−4)	1.76(−3)	8.12(−4)
0.12	3.92(−3)	4.53(−3)	2.60(−3)	4.86(−3)	2.79(−3)
0.14	9.99(−3)	1.02(−2)	6.72(−3)	1.07(−2)	7.07(−3)
0.16	2.07(−2)	1.96(−2)	1.42(−2)	2.05(−2)	1.48(−2)
0.18	3.69(−2)	3.41(−2)	2.63(−2)	3.53(−2)	2.72(−2)
0.20	5.81(−2)	5.50(−2)	4.43(−2)	5.66(−2)	4.56(−2)
0.25	1.42(−1)	1.44(−1)	1.25(−1)	1.47(−1)	1.27(−1)
0.30	2.73(−1)	3.06(−1)	2.75(−1)	3.07(−1)	2.77(−1)
		Niobium ($Z_2=41$, $\omega_K=0.748$)			
0.16	1.40(−4)	2.46(−4)	7.75(−5)	3.03(−4)	9.53(−5)
0.20	1.14(−3)	9.57(−4)	4.43(−4)	1.13(−3)	5.24(−4)
0.24	2.97(−3)	2.60(−3)	1.50(−3)	2.96(−3)	1.71(−3)
0.28	7.37(−3)	5.68(−3)	3.76(−3)	6.27(−3)	4.16(−3)
0.32	1.44(−2)	1.08(−2)	7.81(−3)	1.16(−2)	8.41(−3)
0.36	2.57(−2)	1.83(−2)	1.41(−2)	1.95(−2)	1.50(−2)
0.40	4.04(−2)	2.92(−2)	2.36(−2)	3.05(−2)	2.46(−2)
0.45	7.02(−2)	4.82(−2)	4.05(−2)	4.96(−2)	4.17(−2)
		Silver ($Z_2=47$, $\omega_K=0.830$)			
0.15	4.56(−6)	1.65(−5)	2.03(−6)	2.38(−5)	2.92(−6)
0.20	1.10(−4)	1.39(−4)	3.90(−5)	1.85(−4)	5.20(−5)
0.25	5.10(−4)	5.69(−4)	2.44(−4)	6.95(−4)	2.98(−4)
0.30	1.55(−3)	1.57(−3)	8.58(−4)	1.81(−3)	9.91(−4)
0.35	3.68(−3)	3.44(−3)	2.19(−3)	3.83(−3)	2.43(−3)
0.40	6.73(−3)	6.50(−3)	4.56(−3)	7.04(−4)	4.94(−3)
0.45	1.27(−2)	1.12(−2)	8.41(−3)	1.18(−2)	8.84(−3)
0.50	2.00(−2)	1.77(−2)	1.40(−2)	1.83(−2)	1.45(−2)
0.55	3.14(−2)	2.58(−2)	2.12(−2)	2.70(−2)	2.21(−2)
0.60	4.63(−2)	3.78(−2)	3.19(−2)	3.81(−2)	3.22(−2)
		Antimony ($Z_2=51$, $\omega_K=0.867$)			
0.20	2.03(−5)	3.86(−5)	7.07(−6)	5.67(−5)	1.04(−5)
0.25	1.38(−4)	1.76(−4)	5.59(−5)	2.43(−4)	7.74(−5)
0.30	4.46(−4)	5.27(−4)	2.32(−4)	6.84(−4)	3.01(−4)
0.35	1.18(−3)	1.24(−3)	6.67(−4)	1.51(−3)	8.15(−4)
0.40	2.50(−3)	2.42(−3)	1.50(−3)	2.87(−3)	1.77(−3)
0.45	4.85(−3)	4.27(−3)	2.90(−3)	4.89(−3)	3.32(−3)
0.50	7.59(−3)	6.94(−3)	5.04(−3)	7.73(−3)	5.62(−3)
0.55	1.17(−2)	1.06(−2)	8.12(−3)	1.15(−2)	8.82(−3)
0.60	1.70(−2)	1.54(−2)	1.22(−2)	1.64(−2)	1.31(−2)

[a] The notation 1.58(−4) denotes 1.58×10^{-4}; all theoretical cross sections are the result of integrations with exact limits.

to examine the two Coulomb-deflection calculations more closely. An empirical Coulomb-deflection factor can be derived by dividing the measured cross section by the theoretical prediction of the PSSR. If the theoretical calculation accurately accounts for binding, polarization (negligible here), and relativistic effects, the data are an experimental measure of $C(\pi d\zeta_K q_0)$. Figure 4 shows the plot of these data for all projectiles and targets versus the Coulomb-deflection vari-

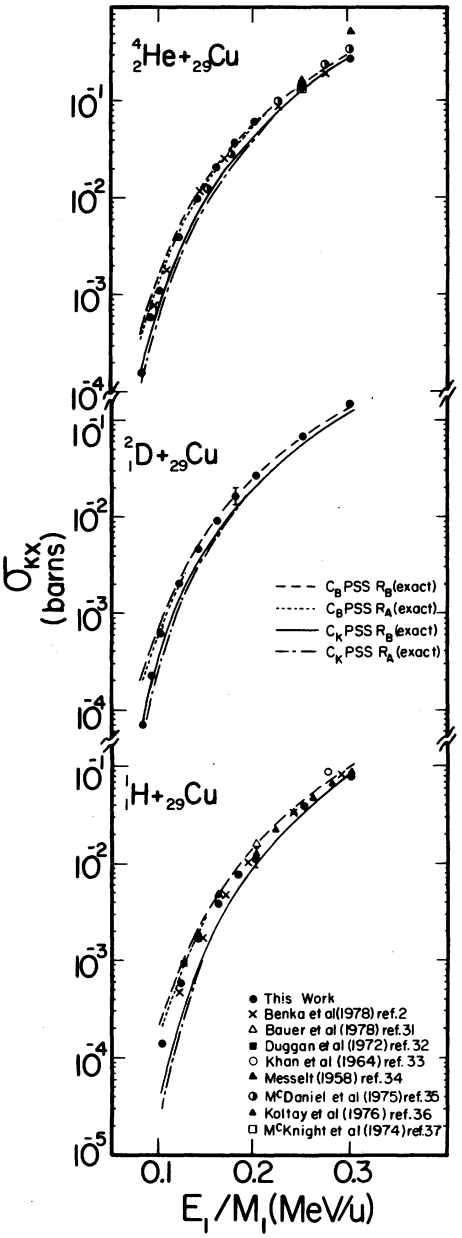

FIG. 2. Measured K-shell x-ray–production cross sections of $_{29}$Cu for proton, deuteron, and alpha particle bombardment. The measured data are compared with other published results and four theoretical calculations.

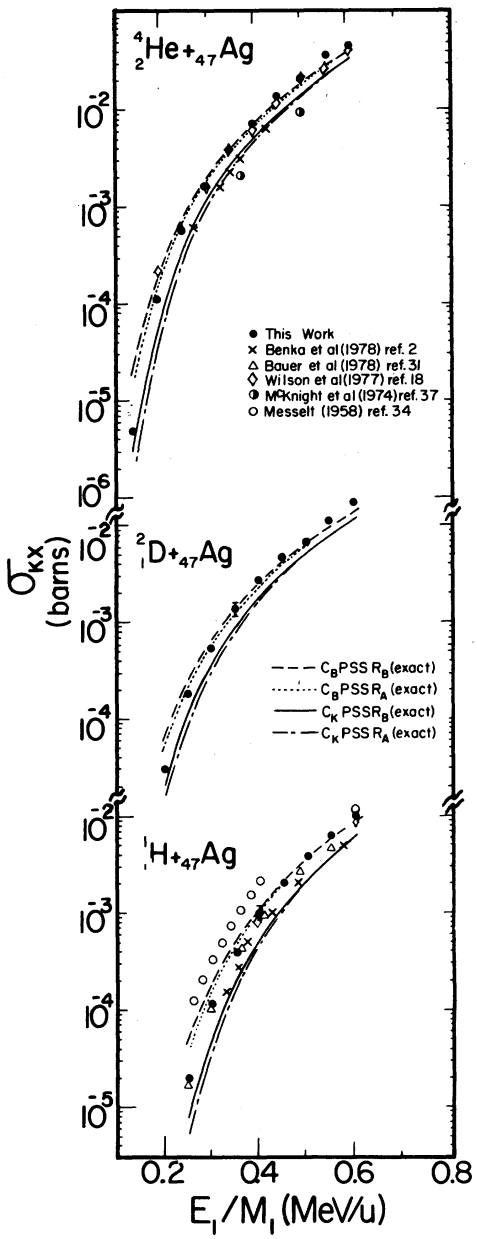

FIG. 3. Measured K-shell x-ray–production cross sections of $_{47}$Ag for proton, deuteron, and alpha particle bombardment. The measured data are compared to other published results and the predictions of four theoretical calculations.

able $\pi d\zeta_K q_0$. The data exhibit universal behavior although the spread in the data is considerably larger than the experimental uncertainties. The locus of the data points is a line on the semi-log plot which crosses $C_B(\pi d\zeta_K q_0)$ at $\pi d\zeta_K q_0 = 0.5$ and has a slope close to that of $C_K(\pi d\zeta_K q_0)$ but is displaced from it by a factor of ~2.5 at $\pi d\zeta_K q_0 = 2.5$ and ~1.3 at $\pi d\zeta_K q_0 = 0.5$. It should be noted that the argument $\pi d\zeta_K q_0$ is calculated using the exact q_0 as pointed out by Lapicki *et al.*[4]

To investigate further the Coulomb-deflection effect, ratios of cross sections for x rays induced by deuterons to those induced by protons at identical velocities were calculated and are plotted

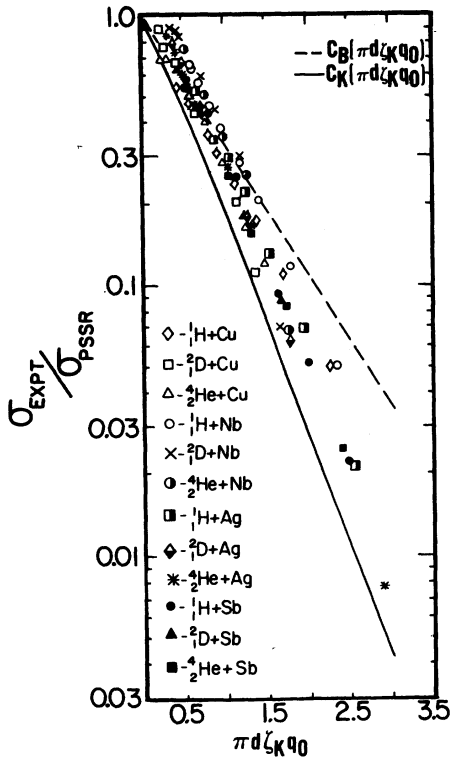

FIG. 4. Empirical Coulomb-deflection factor inferred from measured cross-section values for protons, deuterons, and alpha particles incident on Cu, Ag, Nb, and Sb. These inferred values are compared to the theoretical calculations of Refs. 5 and 6.

in Figure 5. The targets are the same for each projectile. Since $^2_1$D and $^1_1$H have the same Z_1 but different charge to mass ratios, the increased binding effect is the same for both while the Coulomb deflection is not. In addition, experimental normalization factors cancel so that the ratios of measured cross sections are more certain than the cross sections themselves. The difference between calculations made with exact and approximate limits is smaller than experimental uncertainties. These ratios of measured data fall between the predictions of the C_KPSS (exact) and the C_BPSS (exact) as in the case of absolute cross sections. The measured ratio values differ from the theoretical predictions by as much as a factor of 2 at the lowest energies while good agreement with the C_BPSS is found at the highest energies. Relativistic effects cancel in all ratios because the target and projectile velocities are the same for each component.

The ratio of cross sections for $^4_2$He and $^2_1$D projectiles at the same velocity bombarding the same target shows the velocity dependence and relative magnitude of the increased binding effect. The ratio is divided by four to take into account the Z_1^2 dependence given in the PWBA. Since $^4_2$He and $^2_1$D have the same charge to mass ratio the Coulomb-deflection effect is the same for both except for the weak Z_1 dependence introduced through ζ_K in the argument $\pi d\zeta_K q_0$. Figure 6 shows both measured and theoretical values of this ratio for $_{29}$Cu and $_{47}$Ag. The agreement between theory and experiment is quite good and usually within experimental uncertainties. The theoretical ratio values calculated with approximate limits deviate from those calculated with exact limits by less than experimental uncertainties.

VI. CONCLUSIONS

In this work we report the magnitude of the effect of the approximation $\hbar\omega_{2K}/E_{c.m.} \ll 1$, which is used in calculating ionization cross sections in

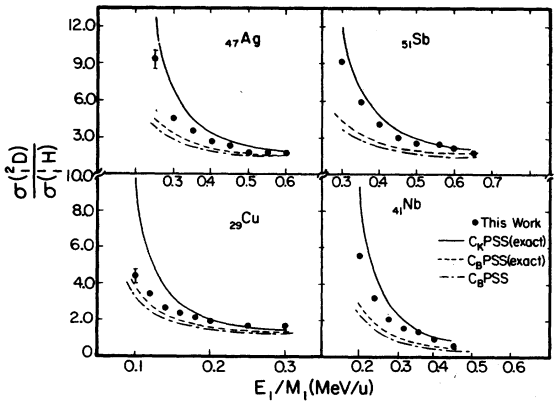

FIG. 5. Ratios of measured cross-section values for deuteron bombardment to those for proton bombardment for Cu, Ag, Nb, and Sb. The ratios of measured values are compared to three theoretical calculations.

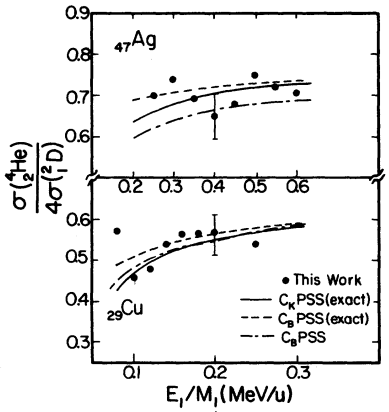

FIG. 6. Ratios of measured cross sections induced by alpha particles to four times those induced by deuterons for $_{29}$Cu and $_{47}$Ag. The ratios of measured values are compared to three theoretical predictions.

the PWBA and PSS theories. Calculations without this approximation obtain values for the ionization cross sections which are lower by ~25%, at $\hbar\omega_{2K}/E_{c.m.} = 0.1$, than calculations in which the approximation is used. Avoiding this approximation introduces a threshold effect which forces the ionization cross section to zero at $E_{c.m.} = \hbar\omega_{2K}$. Experiments designed to explore the low-velocity dependence of ionization cross sections for signs of this threshold effect were carried out using three different projectiles ($^1_1$H, $^2_1$D, and $^4_2$He). This permitted an examination of the data through the formation of cross-section ratios whose values are free of the uncertainties of the various normalization factors which determine absolute values. As a result, an assessment of the theory could be made more sensitively than by a simple comparison of absolute cross sections. Discrepancies much larger than the 25% effect of the approximation were found between theory and experiment in both the magnitude and energy dependence of the absolute cross sections. At these energies, the threshold effect is apparently too small to be measured.

Since both relativistic and Coulomb-deflection effects are very large in this energy region, comparisons were also made with two different calculations of each of these effects. The two relativistic calculations give similar results, but the Coulomb-deflection factors are quite different in both magnitude and energy dependence. In the ratio $\sigma(^2_1\text{D})/\sigma(^1_1\text{H})$, where relativistic and increased binding effects cancel, leaving only the Coulomb-deflection effect, neither theory provides an adequate description of the experimental data. A measurement of the Coulomb-deflection effect, derived using the theoretical predictions for both increased binding and relativistic effects shows the same disagreement with both Coulomb-deflection factors. This suggests that the theoretical predictions for the binding and relativistic effects are at least adequate in both magnitude and energy dependence. The ratio $\sigma(^4_2\text{He})/4\sigma(^2_1\text{D})$, which tests only the binding effect, shows good agreement with theoretical predictions.

ACKNOWLEDGMENTS

This work is supported in part by the Robert A. Welch Foundation, the NTSU Faculty Research Fund, and the Research Corporation. Acknowledgment is made to the donors of the Petroleum Research Fund, administered by the American Chemical Society, for partial support of this research.

---

*Permanent address: Fermi National Laboratory, P. O. Box 500, M. S. # 307, Batavia, Illinois 60510.
†Permanent address: Physical Review Letters, P. O. Box 1000, Ridge, N. Y. 11961.

[1]M. L. Knotek and P. J. Feibelman, Phys. Rev. Lett. 40, 964 (1978).
[2]O. Benka and M. Geretschlager, Z. Phys. A 284, 29 (1978); O. Benka and A. Kropf, At. Data Nucl. Data Tables 22, 219 (1978).
[3]R. Rice, F. D. McDaniel, G. Basbas, and J. L. Duggan, IEEE Trans. Nucl. Sci. NS28, 1103 (1981).
[4]G. Lapicki, R. Laubert, and W. Brandt, Phys. Rev. A 22, 1889 (1980).
[5]W. Brandt, R. Laubert, and I. Sellin, Phys. Lett. 21, 518 (1966); G. Basbas, W. Brandt, and R. Laubert, Phys. Rev. A 7, 983 (1973); 17, 1655 (1978).
[6]L. Kocbach, Phys. Norv. 8, 187 (1976).
[7]R. K. Gardner and T. J. Gray, At. Data Nucl. Data Tables 21, 515 (1978).
[8]H. A. Bethe, Ann. Phys. (N.Y.) 5, 325 (1930); H. A. Bethe, Z. Phys. 76, 293 (1932).
[9]E. Merzbacher and H. Lewis, *Encyclopedia of Physics*, edited by S. Flügge (Springer, Berlin, 1958), Vol. 34, p. 166.
[10]G. S. Khandelwal, B. H. Choi, and E. Merzbacher, At. Data 1, 103 (1969).
[11]J. A. Bearden and A. F. Burr, Rev. Mod. Phys. 39, 125 (1967); W. Lotz, J. Opt. Soc. Am. 60, 206 (1970).
[12]R. Anholt, Phys. Rev. A 17, 976 (1978).
[13]W. Brandt and G. Lapicki, Phys. Rev. A 20, 465 (1979).
[14]J. C. Slater, Phys. Rev. 36, 57 (1930).
[15]R. Rice, G. Basbas, and F. D. McDaniel, At. Data Nucl. Data Tables 20, 503 (1977).
[16]R. Rice, M. S. thesis, North Texas State University, 1977 (unpublished).
[17]J. C. Ashley, R. H. Ritchie, and W. Brandt, Phys. Rev. B 5, 2393 (1972).
[18]S. R. Wilson, F. D. McDaniel, J. R. Rowe, and J. L. Duggan, Phys. Rev. A 16, 903 (1977).
[19]F. D. McDaniel, T. J. Gray, R. K. Gardner, G. M. Light, J. L. Duggan, H. A. Van Rinsvelt, R. D. Lear, G. H. Pepper, J. W. Nelson, and A. R. Zander, Phys. Rev. A 12, 1271 (1975).
[20]J. Tricomi, J. L. Duggan, F. D. McDaniel, P. D. Miller, R. P. Chaturvedi, R. M. Wheeler, J. Lin, K. A. Kuenhold, L. A. Rayburn, S. J. Cipolla, Phys. Rev. A 15, 2269 (1977).
[21]F. D. McDaniel and J. L. Duggan, *Proceedings of the Fourth International Conference on Beam Foil Spectroscopy and Heavy Ion Atomic Physics, Gatlinburg, Tenn., September, 1975*, edited by I. A. Sellin and D. Pegg (Plenum, New York, 1976), Vol. 2, p. 519.
[22]T. J. Gray, P. Richard, R. L. Kauffman, T. C. Holloway, R. K. Gardner, G. M. Light, and J. Guertin, Phys. Rev. A 13, 1344 (1976).
[23]G. Bissinger, P. H. Nettles, S. M. Shafroth, and A. L. Waltner, Phys. Rev. A 10, 1932 (1974).

[24]G. Basbas, *Proceedings of the Fourth International Conference on Scientific and Industrial Applications of Small Accelerators, Denton, Texas, 1976,* edited by J. L. Duggan and I. L. Morgan (IEEE, New York, 1976), p. 142.
[25]F. D. McDaniel, J. L. Duggan, P. D. Miller, and G. D. Alton, Phys. Rev. A 15, 846 (1977).
[26]R. Anholt, Phys. Rev. A 17, 983 (1978).
[27]L. B. Magnusson, Phys. Rev. 107, 161 (1957); R. J. Gehrke and R. A. Lokken, Nucl. Instrum. Methods 97, 219 (1971); J. S. Hansen, J. C. McGeorge, D. Nix, W. D. Schmidt-Ott, I. Unus, and R. W. Fink, *ibid.* 106, 365 (1973); J. L. Campbell and L. A. McNelles, *ibid.* 117, 519 (1974); 125, 205 (1975).
[28]R. Laubert, H. Haselton, J. R. Mowat, R. S. Peterson, and I. A. Sellin, Phys. Rev. A 11, 135 (1975).
[29]J. F. Ziegler, *Hydrogen: Stopping Powers and Ranges in All Elemental Matter* (Pergamon, New York, 1977); J. F. Ziegler, *Helium: Stopping Powers and Ranges in All Elemental Matter* (Pergamon, New York, 1977).
[30]W. Bambynek, B. Craseman, R. W. Fink, J. U. Freund, H. Mark, C. D. Swift, R. E. Price, and P. V. Rao, Rev. Mod. Phys. 44, 716 (1972).
[31]C. Bauer, R. Mann, and W. Rudolph, Z. Phys. A 287, 27 (1978).
[32]J. L. Duggan, W. L. Beck, L. Albrecht, L. Munz, and J. D. Spaulding, *Advances in X-Ray Analysis,* edited by K.-F. J. Heinrich, C. S. Barrett, J. B. Newkirk, and C. O. Ruud (Plenum, New York, 1972), Vol. 15, p. 407.
[33]J. M. Khan and D. L. Potter, Phys. Rev. 133, A890 (1964).
[34]S. Messett, Nucl. Phys. 5, 435 (1958).
[35]F. D. McDaniel, T. J. Gray, and R. K. Gardner, Phys. Rev. A 11, 1607 (1975).
[36]E. Koltay, D. Berenyi, I. Kiss, S. Ricz, G. Hock, and J. Bacso, Z. Phys. A 278, 299 (1976).
[37]R. H. McKnight, R. S. Thornton, and R. L. Karlowicz, Phys. Rev. A 9, 267 (1974).
[38]H. Paul, IEEE Trans. Nucl. Sci. NS28, 1119 (1981).
[39]G. Lapicki and W. Losonsky, Phys. Rev. A 20, 481 (1979).
[40]W. Brandt and G. Lapicki, Phys. Rev. A 20, 465 (1979).